Journal of Solid State Chemistry **142,** 228–235 (1999)
Article ID jssc.1998.8070, available online at http://www.idealibrary.com on IDEAL®

Ab Initio Determination of the Novel Perovskite-Related Structure of $La_7Mo_7O_{30}$ from Powder Diffraction

F. Goutenoire,* R. Retoux,* E. Suard,† and P. Lacorre*,[1]

*Laboratoire des Fluorures, UPRES-A CNRS 6010, Université du Maine, 72085 Le Mans Cedex 9, France; and †Institut Laue Langevin, Avenue des Martyrs, B.P. 156, 38042 Grenoble Cedex 9, France

Received August 5, 1998; accepted October 21, 1998

A new mixed valence molybdate, $La_7Mo_7O_{30}$, first prepared by high energy ball milling, has been successfully synthesized by controlled hydrogen reduction of $La_2Mo_2O_9$. Its original crystal structure was determined from X-ray and neutron powder diffraction (space group R_3; $a = b = 17.0051(2)$ Å, $c = 6.8607(1)$ Å; $Z = 3$; reliability factors: $R_p = 0.081$, $R_{wp} = 0.091$, $\chi^2 = 3.1$, $R_{Bragg} = 0.049$, $R_F = 0.033$). It consists in the hexagonal stacking of individual cylinders of perovskite-type arrangement. These cylinders are built up from perovskite cages sharing corners in trans-position along their diagonal axis. Two different mixed-valence molybdenum sites coexist, with more ($Mo^{+5.75}$) or less ($Mo^{+4.5}$) distorted octahedral environments. Lanthanum atoms are located within the perovskite cages and around them, very close to their regular positions in the perovskite structure. Lanthanum and molybdenum atoms thus form two rows of almost perfect cubes, shifted from each other by $c/2$. An electron microscopy study revealed the defect-free cationic and octahedral arrangements in the (a, b) plane.

Key Words: **ball milling; controlled reduction; reduced lanthanum molybdate; perovskite type rods; structural determination; X-ray and neutron powder diffraction; electron microscopy.**

INTRODUCTION

Studies of rare earth molybdenum oxides have produced a large family of compounds with interesting physical properties (see for instance Refs. (1–8)). These physical properties depend on the structures of these oxides and the oxidation state of molybdenum. For instance, the most oxidized compounds can present ferroelectric properties ($Gd_2Mo_3O_{12}$ (1)) or the more unusual negative thermal expansion ($Ln_2Mo_3O_{12}$ and $Ln_2W_3O_{12}$ (2)). More reduced molybdates present some interesting transport properties such as metal–insulator transitions, for instance $La_2Mo_2O_7$ (3, 4), which exhibits short Mo–Mo distances. This variety of oxidation states, structural arrangements, and properties incited us to explore the condition of stabilization of new reduced rare earth molybdates using various synthesis conditions. In a previous study (9), the possibility has been evidenced of direct synthesis, through high energy ball milling, of a series of lanthanum molybdates with La:Mo ratio 1:1. Among these, a new phase was discovered, with approximate formula $La_2Mo_2O_{8.5-\delta}$. It was assumed to originate from a partial reduction process of the starting $La_2O_3 + 2MoO_3$ mixture by the vial and balls WC surface. We have now confirmed this hypothesis by succeeding in obtaining this new phase through hydrogen reduction of the parent oxidized compound $La_2Mo_2O_9$ (10). The unprecedented crystal structure of this new phase, with exact formula $La_7Mo_7O_{30}$, has been determined using X-ray and neutron powder diffraction. It is presented here, together with an electron microscopy study. To our knowledge it is the first time, at least in oxides, that an entirely new structural type has been stabilized using a direct ball milling synthesis technique.

EXPERIMENTAL

Synthesis

The oxide $La_7Mo_7O_{30}$ can be obtained using two synthetic ways, either from direct high-energy ball milling in a WC vial, or through controlled hydrogen reduction of $La_2Mo_2O_9$. A poorly crystallized sample was obtained after 12 h of ball milling a mixture $La_2O_3 + 2MoO_3$ in a WC vial with 6 WC balls (product mass $\sim$1 g, ball/product mass ratio = 80, speed = 1384 tr/min) on a Fritsch Pulverisette 7 planetary mill (9). The crystallinity can be largely improved by annealing the sample under secondary vacuum ($\approx 10^{-3}$–10^{-4} Pa) during several hours at 800°C. However, the ball milling synthetic method proved to be poorly reproducible, since it was highly dependent on the surface quality of the vial and balls.

Hydrogen reduction of $La_2Mo_2O_9$ (prepared by firing a mixture of $La_2O_3 + 2MoO_3$ for 12 h at 850°C) was

[1]To whom correspondence should be addressed. Fax: +33 2 4383 3506. E-mail: Philippe.Lacorre@univ-lemans.fr.

0022-4596/99 $30.00

performed in a thermogravimetric Setaram TG92 apparatus at a constant temperature of 760°C, under a flow of 6%H_2 and 94%N_2. The TGA curve (see Fig. 1) shows an intermediate stage in the reduction process around 1.5% weight loss, suggesting the existence of a definite phase that is slightly reduced compared to $La_2Mo_2O_9$. The X-ray diffraction pattern of this phase was found to be identical to that of the phase obtained through ball milling. For the neutron diffraction study, a large sample was prepared from several smaller batches. Each reduction was performed with 0.8–1 g of starting oxide heated to 760°C, the temperature being rapidly decreased when the weight loss was approximately 1.5%. This reduction process was performed 10 times to produce 10 g of sample. The sample was finally mixed and heated for homogenization in an evacuated furnace ($\approx 10^{-3}$–10^{-4}Pa) for one night at 800°C. In order to check the stoichiometry of the annealed reduced compound, subsequent re-oxidation in air of a small sample was carried out on a TA Instruments DTA–TGA apparatus (see insert Fig. 1).

Structural Characterization

The X-ray and neutron powder diffraction patterns were recorded on Bragg–Brentano diffractometers (Siemens D500 and ILL D2B, respectively); details of data collection are presented in Table 1. The program Electron Diffraction v3.5 (11), kindly provided by J. P. Morniroli, was used to find the real symmetry of the structure. The atomic arrangement was determined through Patterson function analyses and Fourier syntheses, using alternatively the programs FullProf (12), ShelxS86, and ShelxL93 (13).

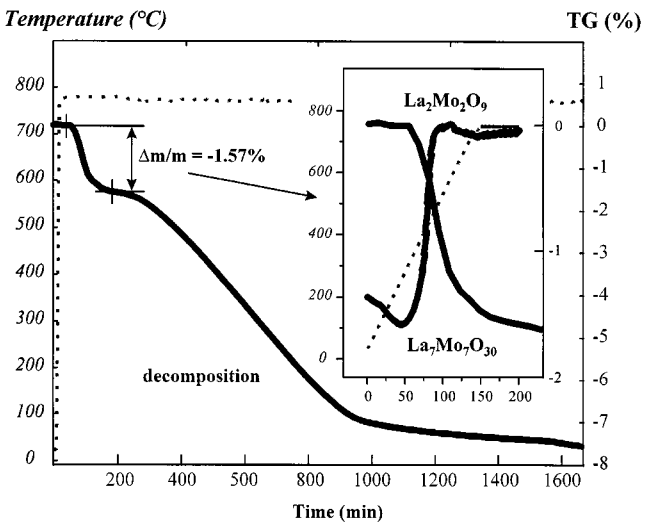

FIG. 1. Thermogravimetric curve of the reduction of $La_2Mo_2O_9$ under diluted hydrogen (6% H_2–94%N_2). In insert: detail of the same curve, together with the thermogravimetric curve of the oxidation of $La_7Mo_7O_{30}$ under a flow of atmospheric air.

TABLE 1
Conditions of X-Ray and Neutron Data Collection and Structural Refinement for $La_7Mo_7O_{30}$

Diffractometer	Siemens D500	D2B (ILL)
Radiation	X-ray Cu$K\alpha$	Neutron 1.5938 Å
2θ range [°]	5–130	5–160
Step-scan increment [°]	0.02	0.05
Counting time	33 s/pt.	3h (total)
Peak shape	Pseudo-Voigt	Pseudo-Voigt
Number of reflections	710	820
Number of refined parameters	35	46
R_{Bragg}	7.16%	4.88%
R_p	11.4%	8.13%
R_{wp}	13.6%	9.10%
R_{exp}	4.18%	5.15%
χ^2	10.7	3.12

The electron diffraction study (high-resolution and diffraction modes) was performed with a JEOL 2010 electron microscope (tilt $\pm$ 30°) fitted with a eucentric goniometer (60°), and equipped with an EDX analyzer. A few droplets of a suspension of microcrystals (obtained from thorough grinding of a powdered sample) in alcohol were deposited on a carbon-coated holey film. The simulated projected potential of the structure was calculated with the series of programs written by P. A. Stadelman (14).

CRYSTAL SYMMETRY

Both X-ray and neutron diffraction patterns of the well-crystallized phases could be perfectly fitted on the base of the monoclinic cell determined from electron diffraction of a poorly crystallized sample (9), with space group $C2/m$ and cell parameters $a = 10.831$ Å, $b = 17.005$ Å, $c = 6.709$ Å, $\beta = 112.03°$. However, a careful examination of both patterns showed that the h and k indices of all observed hkl reflections were even, so that the patterns could be fitted as well into a smaller monoclinic cell with parameters $a =$ 5.4099(2) Å, $b = 8.5026(2)$ Å, $c = 6.7075(2)$ Å, $\beta = 112.021°(1)$. No extra reflection in the X-ray and neutron diffraction patterns could justify the doubling of parameters a and b as observed on electron diffraction patterns.

Direct methods were then applied to the observed intensities as extracted (12) by the program FullProf (Profile Matching mode) on the basis of the small monoclinic cell, using ShelxS86 (13) and Sirpow92 (15). No satisfying solution resulted from the calculation, either in the small or in the large monoclinic cell. This prompted us to reexamine the diffraction patterns. We noticed that some reflections with equal interreticular distances (such as 020, $11\bar{1}$, and $\bar{1}11$ with $d = 4.2503$ Å) had interplanar angles exactly equal to 120°. It strongly suggests that the lattice is hexagonal rather than

monoclinic. As a matter of fact, the X-ray and neutron diffraction patterns could be indexed in a hexagonal cell with parameters $a = 17.0064(2)$ Å and $c = 6.8613(1)$ Å.

Several new reciprocal lattice reconstructions from electron diffraction patterns were made in order to confirm the symmetry. The new reflection conditions found are hkl: $-h + k + l = 3n$, which imply a rhombohedral symmetry. The [001]* and [1$\bar{1}$0]* electron diffraction patterns of $La_7Mo_7O_{30}$ shown in Fig. 2 evidence the $hk0$: $-h + k = 3n$, and hhl: $l = 3n$ conditions.

The electron diffraction pattern presented on Fig. 2b has been indexed with the parameters preliminary found in the X-ray and neutron diffraction study. In that figure, reflection dots can clearly be seen, which imply a doubling of the hexagonal c parameter (small horizontal arrows). Such a doubling could be seen, in the reciprocal lattice reconstructions, on every electron diffraction pattern involving the c axis. However, powder diffraction patterns did not show any notable extra reflection that would induce a doubling of the c axis. Only one or two very faint extra peaks in the X-ray pattern could possibly justify such a doubling, not enough, however, to be taken seriously into account in the search procedure for atomic positioning.

Reflection conditions in the single hexagonal cell suggested a rhombohedral symmetry (cell parameters $a = 10.0807$ Å, $\alpha = 115.012°$) with no extra conditions, thus suggesting $R3$, $R\bar{3}$, $R32$, $R3m$, or, $R\bar{3}m$ as possible space groups.

STRUCTURAL DETERMINATION

The *ab initio* structural determination was carried out in the hexagonal setting of the rhombohedral single cell, starting with the centrosymmetric space groups $R\bar{3}m$ and $R\bar{3}$. The Patterson function was calculated using program ShelxS86 with integrated intensities as extracted, by the full pattern decomposition method of program FullProf, from the X-ray diffraction pattern in order to locate heavy atoms first. The analysis of the Patterson functions and consideration of distances between cations gave us evidence that space group $R\bar{3}$ was the most appropriate. It allowed us to find two atomic positions $M_1 \approx 0.80, 0.00, z + 0.25$, and $M_2 \approx 0.20, 0.00, z$. The rest of the atomic sites were located after subsequent cycles of refinement and Fourier syntheses with programs ShelxL93 and FullProf (refinement mode). At the final stage, all the atomic sites and the isotropic thermal factors of the heavy atoms were refined. In these conditions the lowest R_{Bragg} reliability factor (7.16%) was obtained for the atomic positions listed in Table 2 (see Fig. 3a). In order to get a better precision on the oxygen atoms location, a structural refinement was performed using the neutron diffraction pattern. With all atomic positions and isotropic thermal factors refined, the reliability factor was lowered to $R_{\text{Bragg}} = 4.88\%$ (see Table 2 and Fig. 3b). A refinement in the acentric subgroup $R3$ did not improve this result significantly.

The compound's formula proved to be $La_7Mo_7O_{30}$, with one formula unit in the rhombohedral cell (rhombic description). Thermogravimetric measurements of weight loss and gain from or toward the parent compound $La_2Mo_2O_9$ appeared to be slightly higher ($\sim$1.5%) (see Fig. 1) than expected from the formula ($\sim$1.1%). This slight discrepancy might be due either to the measurement precision or to a slight deficiency on the oxygen lattice. However, subsequent refinements of the occupation rate on oxygen sites (neutron diffraction data) did not show any oxygen deficiency.

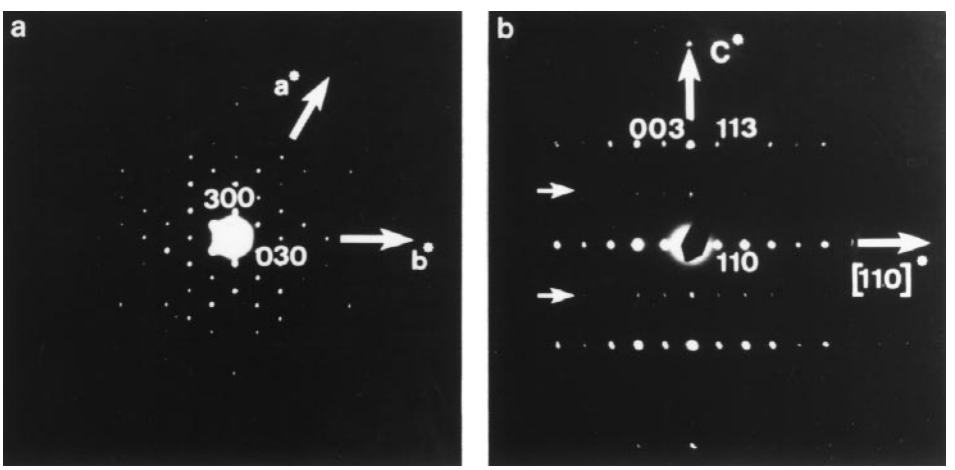

FIG. 2. Electron Diffraction pattern of $La_7Mo_7O_{30}$ along [001]* (a) and [1$\bar{1}$0]* (b) of the hexagonal cell. The ED pattern obtained along [1$\bar{1}$0]* has been indexed with the parameters found in the X-ray and neutron diffraction study. Small horizontal arrows point lines of dots suggesting a doubling of the hexagonal c parameter ($c \approx 13.7$ Å) which has not been taken into account in the structure calculations (see text).

TABLE 2
Crystallographic Parameters[a] of $La_7Mo_7O_{30}$

Atom	Site	x	y	z	B (Å^2)
La1	3a	0	0	0	0.79(9)
					0.62(9)
Mo1	3b	0	0	1/2	0.5(1)
					0.4(1)
La2	18f	0.7803(1)	− 0.0176(2)	0.3345(4)	0.83(4)
		0.7800(1)	*− 0.0167(1)*	*0.3342(4)*	*0.54(3)*
Mo2	18f	0.1992(1)	0.0118(2)	0.1666(4)	0.60(4)
		0.2001(1)	*0.0131(2)*	*0.1660(6)*	*0.42(4)*
O1	18f	0.2423(2)	0.0989(2)	0.3573(4)	0.97(5)
		0.248(1)	*0.089(1)*	*0.343(2)*	*1.00*[b]
O2	18f	0.2931(1)	0.0454(2)	− 0.0006(5)	0.87(5)
		0.293(1)	*0.039(1)*	*− 0.003(2)*	*1.00*[b]
O3	18f	0.1719(2)	0.1153(2)	0.0404(4)	1.12(6)
		0.182(1)	*0.124(1)*	*0.014(3)*	*1.00*[b]
O4	18f	0.2060(2)	− 0.0716(2)	0.3094(4)	*0.85(4)*
		0.204(1)	*− 0.075(1)*	*0.319(2)*	*1.00*[b]
O5	18f	0.0344(2)	0.1043(2)	0.3205(5)	0.67(2)
		0.036(1)	*0.104(1)*	*0.319(2)*	*1.00*[b]

Note. Space group: R_3 (No. 148), rhombic $Z = 1$, hexagonal $Z = 3$. Cell parameters: $a = 17.0051(2)$ Å, $c = 6.8607(1)$ Å, *$a = 17.0064(2)$ Å, $c = 6.8613(1)$ Å*.

[a] Cell parameters and atomic coordinates (from X-ray data: in italic) are given in the hexagonal setting (full occupancy for all sites).

[b] The oxygen thermal factor is arbitrary fixed to 1.0 Å^2.

CATIONS COORDINATION AND VALENCE

The analysis of interatomic distances and angles (Table 3) was based on the atomic parameters as refined from the neutron diffraction data. The La1 coordination polyhedron is a quasi-regular icosahedron (see Fig. 4a), with two groups of close La–O distances: La1–O3 = 2.59 Å and La1–O5 = 2.70 Å. The La2 coordination polyhedron (see Fig. 4a) is more distorted, La2 being surrounded by nine oxygen atoms at distances ranging from 2.44 to 2.85 Å. This polyhedron can be considered as a very distorted monocapped antiprism, but is better described as a nonregular pentagon, dicapped on both sides like in $LaPO_4$. The two capping dioxygen groups form two edges almost perpendicular to each other. Valence calculations for lanthanum atoms give +3.35 and +3.08 for La1 and La2, respectively, slightly in excess of the expected +3.

The Mo1 coordination polyhedron is an almost regular octahedron (Fig. 4b) formed by six oxygen neighbors at equal distance (d(Mo1–O5) = 1.99 Å), with 180° *trans*-oxygen O–Mo–O angles and *cis*-oxygen O–Mo–O angles between 85° and 95°. The Mo2 coordination polyhedron is a more distorted octahedron (Fig. 4b), with Mo–O distances ranging from 1.77 to 2.21 Å, *trans*-oxygen O–Mo–O angles from 152° to 170°, and *cis*-oxygen O–Mo–O angles from 78° to 105°. Such an environment is comparable to that of molybdenum in MoO_3, where distances range from 1.67 to 1.95 Å forming a distorted tetrahedron, with two longer distances at 2.25 and 2.33 Å, altogether forming a very distorted octahedron. Quite similarly, the strongly distorted Mo2 coordination octahedron is formed by four short distances between 1.77 and 1.94 Å, and two longer ones at 2.20 and 2.21 Å.

The more or less distorted octahedral coordination most probably reflects a difference in the oxidation states of the corresponding molybdenum atoms. For instance, Mo^{4+} in oxides is known to have a regular octahedral coordination, while smaller Mo^{6+} has either a very distorted octahedral coordination or a tetrahedral coordination. It is thus tempting to attribute a lower valence to Mo1 than to Mo2, the latter being probably close to +6. In order to estimate the mean oxidation state on each Mo site, a Mo valence calculation was undertaken. Unfortunately, only Mo^{VI} appears in the list of bond-valence parameters compiled by Brese and O'Keeffe in their reference paper (16).

The bond-valence parameters for lower oxidation states of Mo had therefore to be calculated from known structures of reduced molybdates. For the purpose, only known structures with molybdenum sites where an integer oxidation state has been clearly evidenced were considered. This is the case, for instance, of MoO_2 (17), $La_2Mo_2O_7$ (3), $Y_2Mo_2O_7$ (18), $La_5Mo_4O_{16}$ (8), $Mg_2Mo_3O_8$ (19), or $Fe_2Mo_3O_8$ (20) for Mo^{IV}, and of $La_4Mo_2O_{11}$ (21), La_3MoO_7 (5), $La_5Mo_4O_{16}$ (8), or La_2LiMoO_6 (22) for Mo^{V}. From these structures, average bond-valence parameters in oxides were found to be $R = 1.869$ Å and $R = 1.901$ Å for Mo^{IV} and Mo^{V}, respectively. These values compare well with $R = 1.907$ Å for Mo^{VI} given in Ref. (16). They lead to the following average Mo–O distances in regular octahedral coordination: 2.019 Å for Mo^{IV} and 1.969 Å for Mo^{V}. The measured Mo–O distance in the most regular [MoO_6] octahedron of $La_7Mo_7O_{30}$ (Mo1) is intermediate between these two values (1.991 Å), thus suggesting that the oxidation state of Mo1 is between +4 and +5. Assuming a +3 oxidation state for La, the $La_7Mo_7O_{30}$ stoichiometry therefore implies Mo2 to have an oxidation state between +5 and +6. More precisely, if site Mo1 is statistically occupied by $xMo^{V} + (1 - x)Mo^{IV}$, Mo2 has to be statistically occupied by $(1 + x)/6$ $Mo^{V} + (5 - x)/6$ Mo^{VI}. Assuming such a statistical occupation together with the Mo–O distances of Table 3, the Mo theoretical valence was computed as a function of x from the bond-valence parameters of Mo^{VI}, Mo^{V}, and Mo^{IV} as determined above.

Figure 5 gives the result of such a calculation, as the evolution with x of the difference between the calculated valence and the corresponding formal charge ($4 + x$ for Mo1, $(35 - x)/6$ for Mo2). The most appropriate distribution is obtained for a null difference, which appears to be close to $x = 0.5$. The probable mean valences of Mo1 and Mo2 are thus +4.5 and +5.75, respectively.

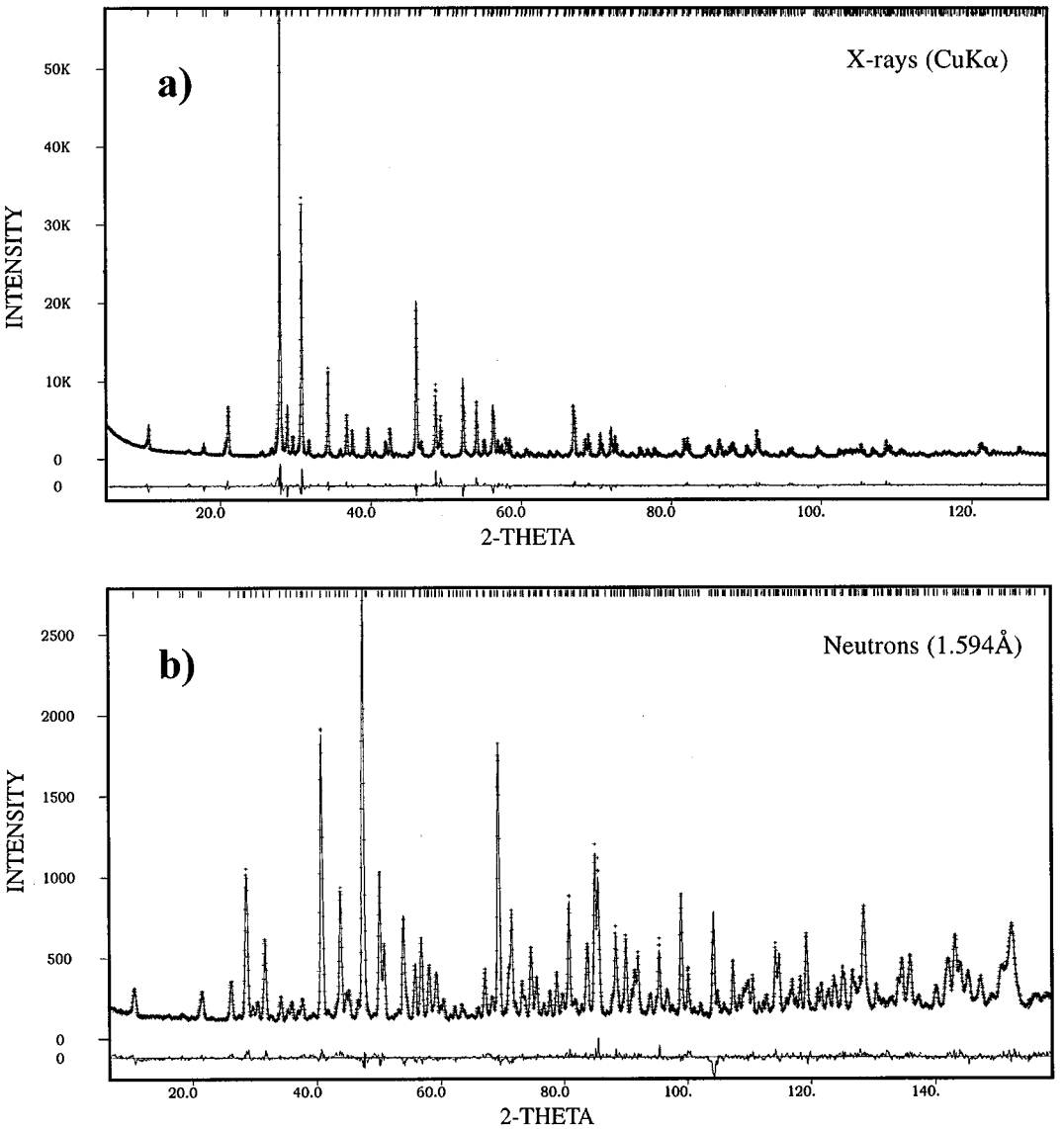

FIG. 3. Result of the structural refinement of $La_7Mo_7O_{30}$: observed (crosses), calculated (line) and difference (lower) profiles for X-ray (a) and neutron (b) diffraction data.

STRUCTURE DESCRIPTION

The most interesting feature of this structure is revealed by the connection between Mo atoms. The closest Mo atoms are very regularly spaced ($d_{Mo-Mo} = 4.009$ Å), with interatomic Mo–Mo–Mo angles very close to 90° (between 89.3° and 90.7°), thus forming almost regular cubes with 4.01 Å edges. The same is true for La atoms with a $c/2$ shift: they form slightly distorted cubes with edges between 4.25 and 4.27 Å and angles between 86° and 94.2°. In each Mo or La set, cubes share corners along their long diagonal, thus forming infinite chains along the c axis of the structure (see Fig. 6a). A close examination of the positioning of oxygen atoms reveals that the molybdenum coordination octahedra form distorted perovkite cages with La1 lanthanum atoms at their center (see Fig. 6b). La2 lanthanum atoms surround the infinite files of perovskite cages in almost the same manner as in the perovskite structure, the lanthanum cubes being only slightly (6.5%) bigger than the molybdenum cubes. Note that alkaline earth molybdates $AMoO_3$ (A = Ca,Sr,Ba) adopt a regular perovskite structure with Mo^{4+}–Mo^{4+} distances close to 4 Å (see (23) and references therein) and that the lanthanum molybdate $La_5Mo_4O_{16}$ (8) exhibits perovskite-type layers.

TABLE 3
Selected Bond Distances (Å) and Angles (°) for $La_7Mo_7O_{30}$

Molybdenum Mo1 (regular octahedron)						
Mo1–O5			1.991(3) [×6]			
O5–Mo1 – O5			94.1(1) [×6]			
O5–Mo1–O5			85.8(1) [×6]			
O5–Mo1–O5			180.0(1) [×3]			
Molybdenum Mo2 (distorted octahedron)						
Mo2	O1	O2	O3	O3	O4	O5
O1	**1.832(4)**	105.3(1)	78.1(2)	152.4(2)	95.3(2)	82.5(1)
O2	2.893(5)	**1.807(4)**	90.5(2)	89.7(1)	101.4(2)	169.6(2)
O3	2.564(5)	2.868(6)	**2.210(5)**	78.8(1)	167.6(2)	83.3(1)
O3	*3.658(5)*	2.642(4)	2.639(5)	**1.935(4)**	104.4(2)	80.4(1)
O4	2.666(5)	2.771(4)	*3.962(6)*	2.932(5)	**1.774(5)**	84.4(1)
O5	2.674(5)	*3.991(5)*	2.676(5)	2.961(4)	2.689(6)	**2.200(4)**
Lanthanum La1 (icosahedron)						
La1–O3			2.595(3) [×6]			
La1–O5			2.699(3) [×6]			
Lanthanum La2						
La2–O1			2.474(4) [×1]			
La2–O1			2.449(4) [×1]			
La2–O2			2.545(4) [×1]			
La2–O2			2.541(4) [×1]			
La2–O3			2.564(4) [×1]			
La2–O4			2.847(4) [×1]			
La2–O4			2.824(4) [×1]			
La2–O4			2.534(5) [×1]			
La2–O5			2.529(4) [×1]			

Note. Standard deviations are given in parentheses and the number of equivalent distances or angles is given in brackets.

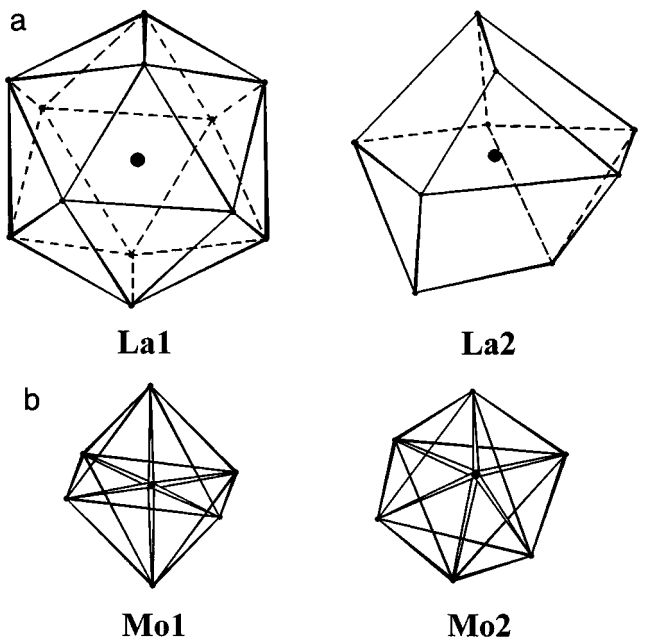

FIG. 4. Coordination polyhedra of the different cations: (a) [La1O_{12}] and [La2O_9], (b) [Mo1O_6] and [Mo2O_6] octahedra.

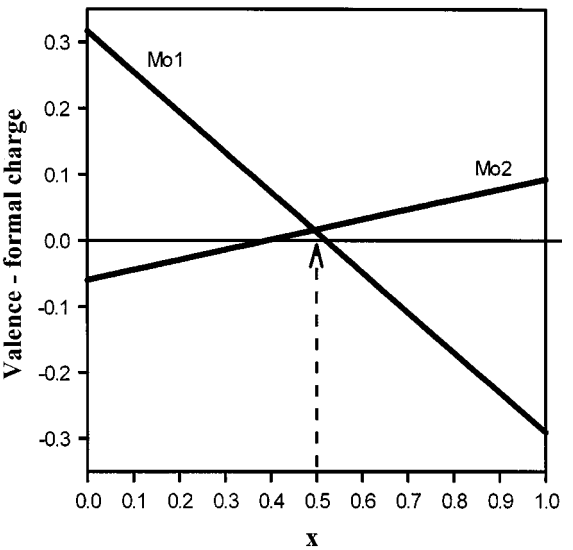

FIG. 5. Difference between valence and formal charge of molybdenum atoms as a function of x, the ratio of Mo^{5+} on site Mo1 (see text for details). The optimum is obtained for $x \approx 0.5$, implying average formal charges close to +4.5 and +5.75 on sites Mo1 and Mo2, respectively.

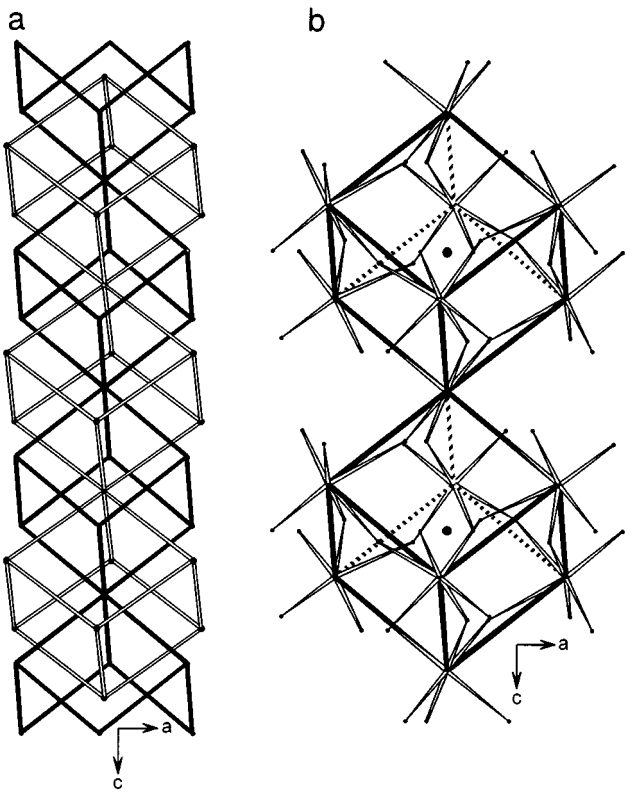

FIG. 6. A perovskite rod or cylinder in $La_7Mo_7O_{30}$: (a) Infinite chain of *trans*-connected Mo (black bonds) and La (open bonds) cubes along the c axis of the structure. (b) Detail of (a): two *trans*-connected Mo cubes with Mo in octahedral coordination forming perovskite cages, with La atoms at their center.

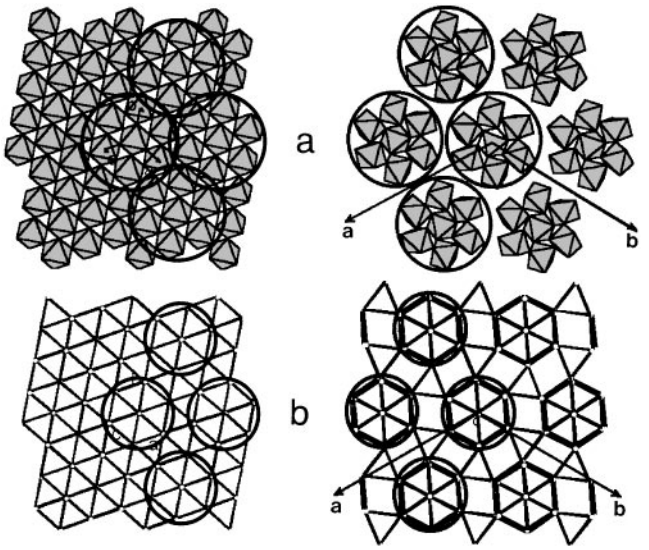

FIG. 7. Projections of the cubic perovskite (left) and $La_7Mo_7O_{30}$ (right) structures along the cubic [111] and hexagonal [001] directions, respectively: (a) octahedral network; (b) cationic network. Large circles represent the sections of perovskite cylinders evoked in the text.

The structure of $La_7Mo_7O_{30}$ is built up from a hexagonal array of cylinders or rods of a perovskite-type arrangement along its three-fold axis (see Fig. 7). A high-resolution electron microscopy image (see Fig. 8) along the c axis of the structure gives a vivid illustration of the very regular cationic arrangement (no defect was observed). Each rod of formula $La_7Mo_7O_{30}$ is shifted by $c/3$ relative to its neighbors. The coordination polyhedron of lanthanum La2 is formed by oxygen atoms belonging to three neighboring perovskite cylinders, thus ensuring the consistency of the structure. On a formal point of view, this $A_7B_7O_{30}$ structure can thus be obtained from that of a perovskite by conveniently inserting nine oxygen atoms around $A_7B_7O_{21}$ cylinders (as previously defined along the perovskite [111] axis) in order to complete B coordination octahedra. The isolated cylinders are slightly rotated around, and shifted along, the cubic [111] or hexagonal c directions.

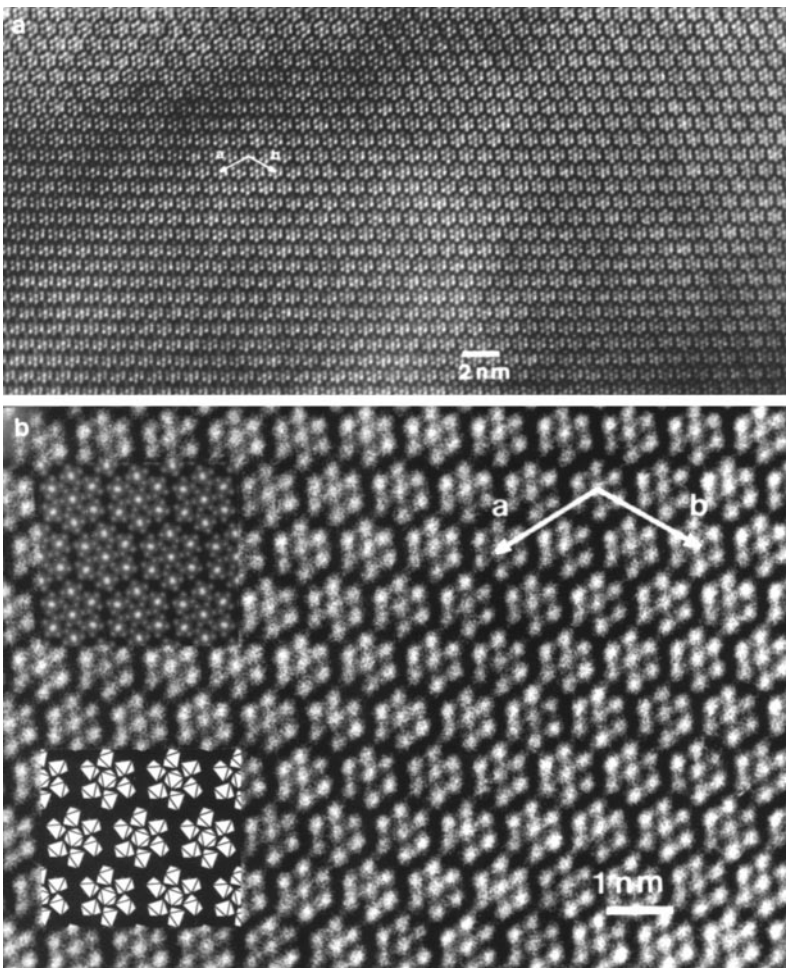

FIG. 8. [001] HREM images of a microcrystal of $La_7Mo_7O_{30}$: (a) very regular contrast throughout the whole crystal, attesting the perfect ionic ordering; (b) detail of (a), with inserted projected potential and structural detail.

SUMMARY AND CONCLUSION

An unprecedented structural type has been obtained in the La–Mo–O system either by energetic ball milling of $La_2O_3 + 2MoO_3$ in WC, or by controlled reduction of $La_2Mo_2O_9$ under hydrogen. To our knowledge, this is the first time that an entirely new crystal structure type has been prepared by ball milling, at least in the oxide field. This structure is built up from hexagonal stacking of isolated perovskite type building units, which can be described as cylinders along the cubic perovskite [111] axis. This is at variance from perovskite-related structures with fourling units (24), whose main axes run along the perovskite [100] direction. As indicated by the stoichiometry ($A_7B_7O_{30}$), the new structure can formally be described as a distorted perovskite arrangement ($A_7B_7O_{21}$) with extra oxygen atoms. Up to now, however, we were not able to obtain a hypothetical $LaMoO_3$ perovskite by reducing $La_7Mo_7O_{30}$.

Since $La_7Mo_7O_{30}$ can be obtained through reduction of $La_2Mo_2O_9$, the question is opened of a possible relationship between the two structural arrangements (of formula $La_{14}Mo_{14}O_{60}$ and $La_{14}Mo_{14}O_{63}$, respectively). A study of the hitherto unknown structural arrangement of $La_2Mo_2O_9$ is currently in progress.

Concerning the charge distribution on molybdenum atoms, one can wonder whether the c axis doubling observed in the electron diffraction study does not reflect a possible charge ordering along the c axis between Mo^{IV} and Mo^{V} on the Mo1 site. Such a partial charge ordering would be consistent with the $+4.5$ mean oxidation state found on this site, and furthermore it would be, as actually evidenced, very hard to detect on powder diffraction patterns. Such a charge ordering could also explain the insulating property of the compound.

ACKNOWLEDGMENTS

The authors express special thanks to Dr. N. Randrianantoandro (Laboratoire de Physique de l'Etat Condensé Université du Maine, Le Mans, France) for access to the planetary mill.

REFERENCES

1. W. Jeitschko, *Acta Crystallogr. Sect. B* **28,** 60 (1972).
2. J. S. O. Evans, T. A. Mary, and A. W. Sleight, *J. Solid State Chem.* **133,** 580 (1997).
3. A. Moini, M. A. Subramanian, A. Clearfield, F. J. DiSalvo, and W. H. McCaroll, *J. Solid State Chem.* **66,** 136 (1987).
4. T. Mingliang, M. Zhiqiang, and Z. Yuheng, *J. Phys. Condensed Matter* **8,** 3413 (1996).
5. J. E. Greedan, N. P. Raju, A. Wegner, P. Gougeon, and J. Padiou, *J. Solid State Chem.* **129,** 320 (1997).
6. H. Kerner-Czeskleba and G. Tourné, *Mater. Res. Bull.* **13,** 271 (1978).
7. J. Gopalakrishnan and A. Manthiram, J. *Chem. Soc. Dalton Trans.* **668,** (1981).
8. M. Ledesert, Ph. Labbé, W. H. McCaroll, H. Leligny, and B. Raveau, *J. Solid State Chem.* **105,** 143 (1993).
9. P. Lacorre and R. Retoux, *J. Solid State Chem.* **132,** 443 (1997).
10. J. P. Fournier, J. Fournier, and R. Kohlmuller, *Bull. Soc. Chim. Fr.*, 4277 (1970)
11. J. P. Morniroli, D. Vankieken, and L. Winter, "Electron Diffraction," Version 3.5.
12. J. Rodriguez-Carjaval, "FullProf," Version 2.6.1, 1994.
13. G. M. Sheldrick, ShelxS86, *in* "Crystallographic Computing 3" (G. M. Sheldrick, C. Krüger, and R. Goddard, Eds.), Oxford Univ. Press, Oxford, 1985; G. M. Sheldrick, "ShelxL93: A Program for Refinement of Crystal Structures from Diffraction Data," Univ. of Göttingen, 1993.
14. P. A. Stadelman, *Ultramicroscopy* **21,** 131 (1987).
15. A. Altomare, G. Cascarano, G. Giacovazzo, A. Guagliardi, M. C. Burla, G. Polidori, and M. Camalli, *J. Appl. Crystallogr.* **27,** 435 (1994).
16. N. E. Brese and M. O'Keeffe, *Acta Crystallogr. Sect. B* **47,** 192 (1991).
17. B. G. Brandt and A. C. Skapski, *Acta Chem. Scand.* **21,** 661 (1967); B. G. Brandt, *Chem. Commun.* (*Univ. Stockholm*), 1 (1971); A. A. Bolzan, B. J. Kennedy, and C. J. Howard, *Aust. J. Chem.* **48,** 1473 (1995).
18. J. N. Reimers, J. E. Greedan, and M. Sato, *J. Solid State Chem.* **72,** 390 (1988).
19. R. Knorr and U. Mueller, *Z. Anorg. Allg. Chem.* **621,** 541 (1995).
20. Y. Le Page and P. Strobel, *Acta Crystallogr. Sect. B* **38,** 1265 (1982); Y. Kanazawa and A. Sasaki, *Acta Crystallogr. Sect. C* **42,** 9 (1986).
21. P. Gall and P. Gougeon, *Acta Crystallogr. Sect. C* **48,** 1915 (1992).
22. J. Tortelier and P. Gougeon, *Acta Crystallogr. Sect. C* **52,** 500 (1996).
23. J. B. Goodenough and J. M. Longo, "Landolt-Börnstein," (K.-H. Hellwege and A. M. Hellwege, Eds.), New Series, Group III, Vol. 4a, Chap. 3. Springer-Verlag, Berlin/Heidelberg/New York, 1970, S. Nomura, "Landolt-Börnstein," (K.-H. Hellwege and A. M. Hellwege, Eds.), New Series, Group III, Vol. 12a, Chap. 2. Spinger-Verlag, Berlin/Heidelberg/New York, 1978.
24. B.-O. Marinder, *Acta Chem. Scand.* **45,** 659 (1991).